Gastroenterology 2019;156:1483–1495

Neuronal Development and Onset of Electrical Activity in the Human Enteric Nervous System

Conor J. McCann,[1] Maria M. Alves,[2] Erwin Brosens,[2] Dipa Natarajan,[1] Silvia Perin,[1] Chey Chapman,[1] Robert M. Hofstra,[1,2] Alan J. Burns,[1,2] and Nikhil Thapar[1,3,4]

[1]Stem Cells and Regenerative Medicine, UCL Great Ormond Street Institute of Child Health, London, UK; [2]Department of Clinical Genetics, Erasmus University Medical Center, Rotterdam, The Netherlands; and [3]Prince Abdullah Ben Khalid Celiac Research Chair, College of Medicine, King Saud University, Riyadh, KSA; and [4]Department of Gastroenterology, Great Ormond Street Hospital, London, UK

BACKGROUND & AIMS: The enteric nervous system (ENS) is the largest branch of the peripheral nervous system, comprising complex networks of neurons and glia, which are present throughout the gastrointestinal tract. Although development of a fully functional ENS is required for gastrointestinal motility, little is known about the ontogeny of ENS function in humans. We studied the development of neuronal subtypes and the emergence of evoked electrical activity in the developing human ENS. **METHODS:** Human fetal gut samples (obtained via the MRC-Wellcome Trust Human Developmental Biology Resource–UK) were characterized by immunohistochemistry, calcium imaging, RNA sequencing, and quantitative real-time polymerase chain reaction analyses. **RESULTS:** Human fetal colon samples have dense neuronal networks at the level of the myenteric plexus by embryonic week (EW) 12, with expression of excitatory neurotransmitter and synaptic markers. By contrast, markers of inhibitory neurotransmitters were not observed until EW14. Electrical train stimulation of internodal strands did not evoke activity in the ENS of EW12 or EW14 tissues. However, compound calcium activation was observed at EW16, which was blocked by the addition of 1 μmol/L tetrodotoxin. Expression analyses showed that this activity was coincident with increases in expression of genes encoding proteins involved in neurotransmission and action potential generation. **CONCLUSIONS:** In analyses of human fetal intestinal samples, we followed development of neuronal diversity, electrical excitability, and network formation in the ENS. These processes are required to establish the functional enteric circuitry. Further studies could increase our understanding of the pathogenesis of a range of congenital enteric neuropathies.

Keywords: Fetus; Embryology; Intestine; Fetal.

The enteric nervous system (ENS), the largest branch of the peripheral nervous system, is composed of complex networks of neurons and glia, which are present throughout the gastrointestinal tract.[1] The ENS is derived primarily from vagal neural crest cells,[2] which enter the foregut at embryonic day (E) 9 in mice and migrate in a rostrocaudal fashion to colonize the entirety of the developing gut by E14.[3,4] In avian and mouse models, a smaller population of sacral neural crest–derived cells has also been shown to contribute to the developing ENS in the terminal hindgut.[2,5] During ENS development, enteric neural crest cells (ENCCs) proliferate and migrate extensively in a highly complex manner, with elongation of migratory chains of ENCCs throughout the gut, including transmesenteric migration pathways that have been shown in the mouse.[6] Recent murine work has proposed that topographically, the ENS is built from parallel, overlapping columns of clonally derived ENCCs. Such topographic organization relies on residual founder ENCCs at the level of the myenteric plexus, which give rise to progeny that extend through the width of the gut wall and are arranged along the serosa-mucosa axis.[7] Previous work has shown the spatiotemporal development of neuronal subtypes in the mouse gut, with the appearance of nitrergic neuronal nitric oxide synthase–expressing neurons at approximately E12.5[8] and subsequent development of cholinergic neurons expressing choline acetyltransferase (ChAT) at E14.5.[9] Furthermore, physiological studies in the murine colon have shown the emergence of spontaneous calcium transients in ENCCs at the migratory wavefront at E12.5[10] and the emergence of induced electrical activity in colonic networks at approximately E15.5.[11]

Despite these significant advances in our knowledge regarding the development of the ENS in animal models, insight to many of these developmental milestones in the human ENS is lacking. Previous work has provided evidence of similar rostrocaudal colonization in the human gut, whereby ENCCs enter the foregut at embryonic week (EW) 4 and migrate in an oro-anal fashion to fully colonize the length of the gut by EW7.[12,13] After ENCC colonization, development and maturation of the tunica muscularis occurs, with rostrocaudal differentiation of the smooth muscle layers and development of interstitial cell of Cajal networks.[13] Hence, at approximately EW11, the human colon has adopted an

Abbreviations used in this paper: **ChAT, choline acetyltransferase; E, embryonic day; ENCC, enteric neural crest cell; ENS, enteric nervous system; EW, embryonic week; nNOS, neuronal nitric oxide synthase; qRT-PCR, quantitative real-time polymerase chain reaction; Sub P, substance P; TTX, tetrodotoxin; VAChT, vesicular acetylcholine transporter; VIP, vasoactive intestinal peptide.**

Most current article

0016-5085/$36.00
https://doi.org/10.1053/j.gastro.2018.12.020

WHAT YOU NEED TO KNOW

BACKGROUND AND CONTEXT

Despite advances in our knowledge regarding the functional development of the gut nervous system in animal models, much of the knowledge regarding this process in humans is still lacking.

NEW FINDINGS

The researchers defined the development of a number of nerve cells and the onset of electrical activity within the developing human gut nervous system.

LIMITATIONS

This study relied on small sample sizes for each timepoint examined, due to the scarcity of human fetal gut material.

IMPACT

These findings provide a timeframe for the development of a functional gut nervous system, within human gestation, which was previously unknown.

anatomically mature phenotype. These studies established the critical time frame for colonization and development of the ENS in human fetal gut tissues. However, there is a paucity of evidence regarding the development of neuronal subtypes or of coordinated electrical activity in the human ENS, which are vital processes for the establishment of the normal functional circuitry that underpins neuromuscular function of the gastrointestinal tract.

Here, we show that the spatiotemporal development of multiple enteric neuronal subtypes in the human fetal colon occurs in the early second trimester. We further show the onset of coordinated neural activity in the human enteric neural network and show that this activity is coincident with increases in expression of various genes involved in neurotransmission and action potential generation. Thus, we propose that the period from the late first trimester to the early second trimester is crucial for the development of a repertoire of enteric neural subtypes and to the establishment of a functional ENS.

Methods

Human Samples

Human fetal colonic samples were obtained via the Joint MRC/Wellcome Trust Human Developmental Biology Resource under informed ethical consent with Research Tissue Bank ethical approval (08/H0712/34+5 and 08/H0906/21+5).

Immunohistochemistry

Immunohistochemistry was performed on fetal whole-mount colonic segments and cryostat sections, as previously described[14] (see Supplementary Materials and Methods) by using the primary and secondary antibodies listed in Supplementary Tables 1 and 2, respectively.

Calcium Imaging

Fetal intestinal samples were obtained as previously described, and calcium imaging was performed as previously reported.[15] After tissue excision and preparation (see Supplementary Materials and Methods), electrical train stimulation (2 s, 20 Hz of 300-μs electrical pulses) (Electronic Stimulator 1001; ADInstruments, Oxford, UK) was applied via a platinum/iridium electrode, and images were collected with OptoFluor software (Cairn Research Limited, Faversham, UK).

RNA Extraction and Sequencing

Total RNA from the hindgut of 1 individual embryo from each time point (EW12, EW14, and EW16) was extracted with the RNeasy kit and protocol (Qiagen, Venlo, The Netherlands). RNA quantity and quality were determined using the Lab-on-Chip RNA 6000 Nano (Agilent Technologies, Santa Clara, CA) on the Agilent 2100 Bioanalyzer. Library preparation of 3 technical replicates per developmental time point per embryo was performed on an Illumina HiSeq 4000 (150-base pair paired-end reads), according to the Illumina TruSeq Stranded mRNA Library Prep Kit protocol (Illumina, San Diego, CA). RNA sequencing analysis, candidate gene expression evaluation, and causal network analysis were performed as outlined in Supplementary Materials and Methods.

Quantitative Real-Time Polymerase Chain Reaction

Complementary DNA was prepared from hindgut samples of 3 embryos from each time point (EW12, EW14, and EW16), and quantitative real-time polymerase chain reaction (qRT-PCR) was performed on each sample with technical triplicates, as described before.[16] Expression levels were normalized with 2 housekeeping genes (*ACTB* and *GAPDH*) and averaged. The primers used are described in Supplementary Table 3.

Statistical Analysis

Data are expressed as mean ± standard error of the mean. Differences in the data were evaluated between groups using 1-way analysis of variance (ANOVA), and intergroup differences were determined by Tukey test or unpaired Student t test. P values $< .05$ were taken as statistically significant. The n values reported refer to the number of individual fetal colonic segments used for each protocol.

Results

Development and Maturation of Key ENS Cell Types

To assess the development and maturation of the human fetal ENS, immunohistochemistry was performed on proximal colonic cryosections at EW12–16. This approach and time frame allowed for fate mapping of typical ENS cell types, including enteric neurons and glia, in the second trimester. Human fetal colonic samples at EW12 displayed robust neuron-specific TuJ1 expression, highlighting the presence of enteric neurons. The TuJ1$^+$ cells, termed *neurons* from here on, were located in multiple discrete ganglia-like structures at the level of the myenteric plexus

(Figure 1*A* and *D*, *arrows*). Few TuJ1$^+$ neurons were identified in the submucosal layer at EW12 (Figure 1*A* and *D*, *arrowheads*). At this stage, SM22 staining, a marker of mature smooth muscle, showed 2 distinct muscle layers (Figure 1*A* and *D*), the inner circular layer (Figure 1*D*, *asterisk*) and outer longitudinal layer (Figure 1*D*, *hash*), reflective of the morphology of the mature human enteric neuromusculature. Further maturation of the tunica muscularis was observed with thickening of muscle layers at EW14 (Figure 1*B* and *E*) and EW16 (Figure 1*C* and *F*). Maturation and thickening of the circular muscle was more apparent across this time frame, with SM22$^+$ smooth muscle cells adopting a more uniform phenotype, with elongated nuclei in the circumferential orientation (Figure 1*E* and *F*, *asterisk*). Maturation of the ENS was also observed by EW14, as TuJ1$^+$ ganglia in the myenteric plexus gradually coalesce and increase in size by EW14 (Figure 1*B* and *E*, *arrows*). At this stage, more robust TuJ1$^+$ expression was identified in the submucosal layer, forming a rudimentary and interrupted submuscosal plexus (Figure 1*B* and *E*, *arrowheads*), with neuronal projections extending into mucosal villi. At EW16, TuJ1$^+$ expression and localization were still observed in the myenteric plexus, with further restriction of ganglia-like structures (Figure 1*C* and *F*, *arrows*). Further development of TuJ1$^+$ neurons in the submucosal regions showed a more continuous submucosal plexus (Figure 1*C* and *F*, *arrowheads*), and TuJ1$^+$ neuronal projections were also observed extending into mucosal villi.

To assess the development of enteric glial cells, expression of S100 was examined with immunohistochemistry over a similar time frame. At EW12, S100 expression was observed in the myenteric plexus alongside robust TuJ1 expression (Figure 2*A*, *D*, and *G*, *arrows*). Such S100 expression appeared in isolation at this stage, with little coexpression of TuJ1 in either the myenteric plexus or submucosal layer (Figure 2*A*, *D*, *G*, *arrows*). At EW14, occasional and weak coexpression of S100 and TuJ1 was observed in some cells, both in the myenteric ganglia (Figure 2*B*, *E*, and *H*, *arrows*) and in the submucosal layer (Figure 2*B*, *E*, and *H*, *arrowheads*). Weak S100 expression was additionally observed as a diffuse single cell layer on the serosal surface of EW14 tissue (Figure 2*B*, *E*, and *H*, *hash*). However, by EW16, this diffuse serosal S100 expression was no longer evident, and both S100$^+$ glia (Figure 2*C*, *F*, and *I*, *arrowheads*) and TuJ1$^+$ neurons (Figure 2*C*, *F*, and *I*, *arrows*) were observed discretely in close apposition in myenteric ganglia and in the submucosal plexus with little coexpression.

Neuronal Subtype Development in the Human ENS

Having shown the development of enteric neurons and glia, as well as the maturation of ganglia from EW12 to EW16, we further assessed the development of specific neuronal subtypes in the human fetal colon. Immunohistochemistry of proximal colonic sections at EW12 showed

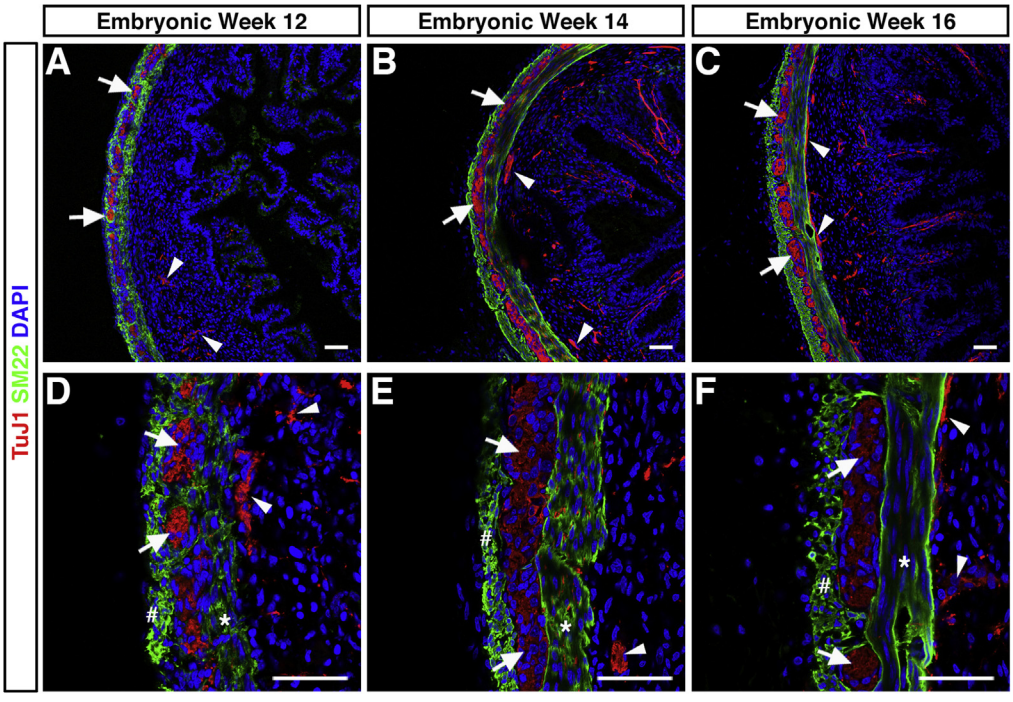

Figure 1. Development and maturation of the enteric neuromusculature in the human fetal colon. (*A–C*) Representative cryosection images at (*A*) EW12, (*B*) EW14, and (*C*) EW16 showing the expression of TuJ1 (*red*), SM22 (*green*), and DAPI (*blue*). TuJ1$^+$ neurons were identified in the myenteric plexus (*arrows*) and in the submucosal region (*arrowheads*). (*D–F*) High-power images of (*D*) EW12, (*E*) EW14, and (*F*) EW16 showing the expression of TuJ1 (*red*), SM22 (*green*), and DAPI (*blue*). TuJ1$^+$ neurons were identified in the myenteric plexus (*arrows*) between the other longitudinal muscle (#) and inner circular muscle (*) layers together and in the submucosal region (*arrowheads*). Scale bars, 50 μm. DAPI, 4′,6-diamidino-2-phenylindole.

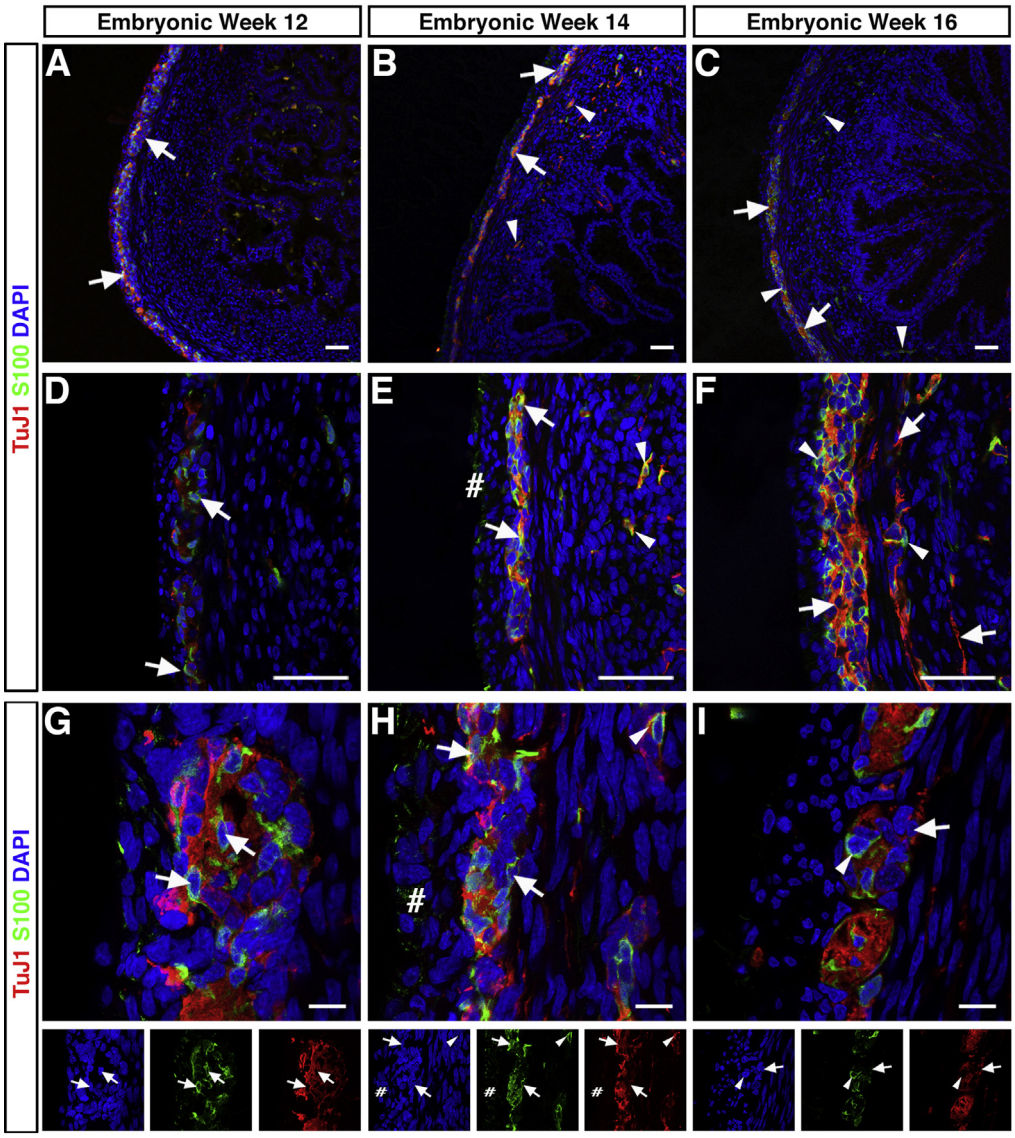

Figure 2. Development and maturation of the enteric glia in the human fetal colon. (*A–F*) Representative cryosection images at (*A–C*) low, (*D–F*) medium, and (*G–I*) high power at (*A*, *D*, *G*) EW12, (*B*, *E*, *H*) EW14, and (*C*, *F*, *I*) EW16 showing the expression of TuJ1 (*red*), S100 (*green*), and DAPI (*blue*). (*A*, *D*, *G*) At EW12, $S100^+$ glial cells were identified in the myenteric plexus (*arrows*) in isolation, with little coexpression of TuJ1. (*B*, *E*, *H*) At EW14, occasional and weak coexpression of S100 and TuJ1 was observed in myenteric ganglia (*arrows*) and in the submucosal layer (*arrowheads*). Weak S100 expression was also observed as a diffuse layer on the serosal surface (#). (*C*, *F*, *I*) At EW16, discrete $S100^+$ glia (*arrowheads*) and $TuJ1^+$ neurons (*arrows*) were observed in myenteric ganglia and in the submucosal plexus. Scale bars, 50 μm (*A–F*), 25 μm (*G–I*). DAPI, 4′,6-diamidino-2-phenylindole.

coexpression of TuJ1 and vesicular acetylcholine transporter (VAChT) (Figure 3*A* and Supplementary Figure 1*A*, *arrows*) and substance P (Sub P) in ganglia-like structures in the myenteric plexus (Figure 3*D* and Supplementary Figure 2*A*, *arrows*). Robust $VAChT^+$ expression was observed in myenteric ganglia (Figure 3*B* and *C* and Supplementary Figure 1*B* and *C*, *arrows*) and in the submuscosal region (Figure 3*B* and *C*, *arrowheads*) at both EW14 and EW16, respectively. Sub P was also observed to be more robustly expressed in myenteric ganglia (Figure 3*E* and *F* and Supplementary Figure 2*B* and *C*, *arrows*) and in the submuscosal region at EW14 and EW16 (Figure 3*E* and *F*, *arrowheads*). Examination of inhibitory neuronal subtypes showed no neuronal nitric oxide (nNOS) (Figure 3*G* and Supplementary Figure 3*A*) or vasoactive intestinal peptide (VIP) (Figure 3*J* and Supplementary Figure 4*A*) expression in EW12 colonic sections, despite robust $TuJ1^+$ expression in the myenteric plexus. By EW14, $TuJ1^+$ neurons were visualized both in the submucosal region and extending into mucosal villi (Figure 3*H*, *arrowheads*), but the $nNOS^+$ neurons were largely restricted to the myenteric plexus (Figure 3*H* and Supplementary Figure 3*B*, *arrows*) at this stage. Similarly, VIP colabeled $TuJ1^+$ neurons at the level of the myenteric plexus at EW14 (Figure 3*K* and Supplementary Figure 4*B*, *arrows*). However, VIP^+ neurons were also visualized in the submucosal region at this stage and extended processes into mucosal villi. With further development to EW16, more extensive $nNOS^+$ (Figure 3*I* and Supplementary Figure 3*C*, *arrows*) and VIP^+ (Figure 3*L* and Supplementary Figure 4*C*, *arrows*) expression was observed at the level of the myenteric plexus. $nNOS^+$ neurons at EW16 appeared to remain restricted to the myenteric region, with little coexpression in $TuJ1^+$ neurons throughout the remaining gut wall (Figure 3*I*, *arrowheads*). By contrast, strong VIP^+ expression was observed in the submucosal region and in villus structures at EW16 (Figure 3*L*, *arrowheads*). Taken together, these data suggest that the initial development of excitatory neurons (VAChT

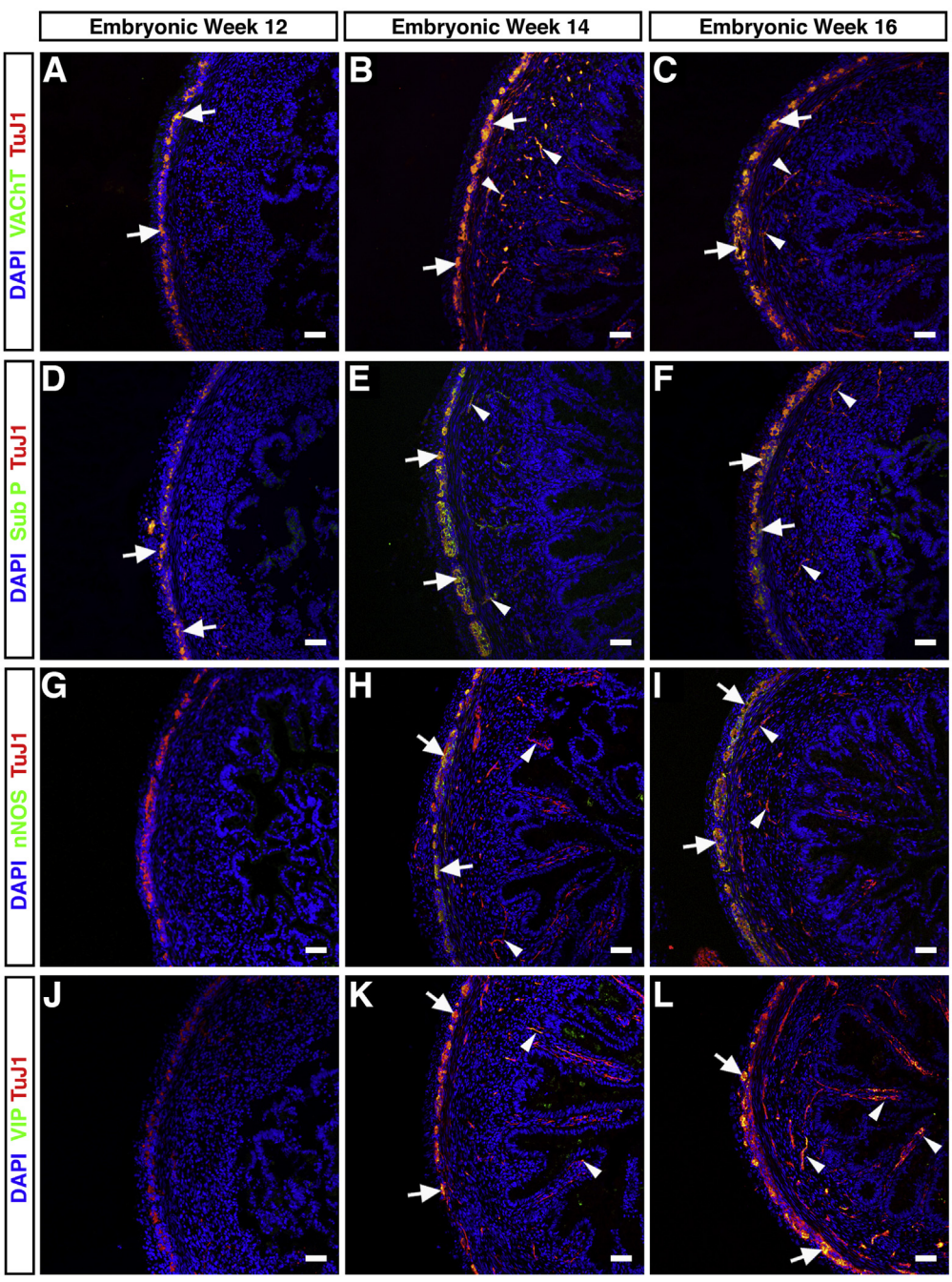

Figure 3. Birth-dating of neuronal subtypes within the human fetal colon. (*A–C*) Representative immunofluorescent images showing expression of TuJ1 (*red*), VAChT (*green*), and DAPI (*blue*). At (*A*) EW12, coexpression of TuJ1 and VAChT was observed in the myenteric plexus (*arrows*) alone. At (*B*) EW14 and (*C*) EW16, coexpression was observed in the myenteric plexus (*arrows*) and in the submucosal region (*arrowheads*). (*D–F*) At (*D*) EW12, coexpression of TuJ1 and Sub P was observed in the myenteric plexus (*arrows*) alone. However, robust coexpression was observed in the myenteric plexus (*arrows*) and in the submucosal region (*arrowheads*) at (*E*) EW14 and (*F*) EW16. (*G–I*) At (*G*) EW12, expression of nNOS was not observed alongside TuJ1 in any region across the gut wall. At (*H*) EW14, coexpression of nNOS and TuJ1 was restricted to the myenteric plexus (*arrows*). $TuJ1^+$ neurons were observed in the submuscosal region extending into the villus crypts. These $TuJ1^+$ neurons did not express nNOS. At (*I*) EW16, nNOS and TuJ1 coexpression was restricted in the myenteric plexus (*arrows*), with little nNOS coexpression in $TuJ1^+$ neurons throughout the remaining gut wall (*arrowheads*). (*J–L*) TuJ1 expression was found in the myenteric plexus and sparsely in the submucosal region at (*J*) EW12 in the absence of VIP staining. At (*K*) EW14, coexpression of nNOS and TuJ1 was observed in the myenteric plexus (*arrows*) and the submuscosal region and extending into the villus crypts (*arrowheads*). At (*L*) EW16, robust nNOS and TuJ1 coexpression was present in the myenteric plexus (*arrows*), the submuscosal region, and extending into the villus crypts (*arrowheads*). Scale bars, 50 μm. DAPI, 4′,6-diamidino-2-phenylindole.

and Sub P) in the human fetal colon occurs before EW12, whereas the development of inhibitory neurons (nNOS and VIP) occurs later, between EW12 and EW14.

Having shown the maturation of the fetal ENS using cryosections, including the birth-dating of neuronal subtypes, we further assessed neural development in whole-mount colonic preparations. Similar to cryosections, immunohistochemistry of EW12 whole-mount colonic preparations showed robust TuJ1$^+$ neural networks at the level of the myenteric plexus. Here, TuJ1$^+$ neurons were observed in complex anastomosing networks with ganglia-like structures (Figure 4*A*, *arrows*) and interganglionic neuronal connections (Figure 4*B*, *arrowheads*). At EW14 (Figure 4*B*) and EW16 (Figure 4*C*), TuJ1$^+$ immunohistochemistry showed further network maturation, including the development of dense neural connections (Figure 4*B* and *C*, *arrows*) and the formation of discrete ganglion structures (Figure 4*B* and *C*, *arrowheads*).

Development of Coordinated Electrical Activity in the Human ENS

To assess the development of coordinated electrical activity in fetal tissues, calcium imaging of whole-mount colonic preparations was performed from EW12 to EW16. Little basal activity was observed in the presumptive ENS of EW12, EW14, or EW16 colonic preparations. However, occasional calcium transients in underlying smooth muscle cells were observed in basal conditions (Supplementary Movies 1–3). Upon electrical point stimulation, no stimulation-induced calcium transients were observed in 3 of 3 EW12 colonic samples ($\Delta F/F_0 = 1.033 \pm 0.002$, n = 3) (Figure 4*D*, *G*, *J*, *M*, and *N* and Supplementary Movie 1). Similarly, electrical stimulation did not elicit calcium transients in fetal tissues in most (4/5) EW14 preparations ($\Delta F/F_0 = 1.055 \pm 0.029$, n = 5, $P = .813$ by Tukey test) (Figure 4*E*, *H*, *K*, *M*, and *N* and Supplementary Movie 2). By EW16, there were statistically significant differences in mean values of stimulation-induced calcium transients between control EW12, EW14, and EW16 groups, as determined by 1-way analysis of variance (ANOVA) ($F_{2,8} = 11.36$, $P = .0046$), with 3 of 3 EW16 colonic preparations displaying compound activation of the ENS (1.211 ± 0.026, n = 3) (Figure 4*F*, *I*, *L*, *M*, and *N* and Supplementary Movie 3) compared with either EW12 ($P = .007$, Tukey test) or EW14 ($P = .008$, Tukey test). Additionally, this stimulation-induced activation of enteric neuronal networks at EW16 was found to be blocked (3/3) in the presence of 1 μmol/L tetrodotoxin (1.029 ± 0.012, n = 3), compared with stimulation in control conditions (1.211 ± 0.026; n = 3; $P = .0028$, Student *t* test) (Figure 4*O* and Supplementary Movie 4). This result suggests the presence of voltage-dependent sodium channels in the ENS at EW16 of human development.

To determine if the stimulation-induced compound activation observed at this stage could be due to the development of synaptic connectivity, we performed immunohistochemistry for synaptophysin across each of the time points examined. At EW12, coexpression of TuJ1 and synaptophysin was observed (Figure 5*A*, *arrows*) in ganglia-like structures of the myenteric plexus. This coexpression was maintained at both EW14 and EW16 (Figure 5*B* and *C*, *arrows*), with additional coexpression visualized in the submuscosal region (Figure 5*B* and *C*, *arrowheads*). These results suggest that although synaptic protein expression is in place by EW12, the development of simulation-induced coordinated electrical activity is not established until later in development, between EW14 and EW16. To investigate whether postsynaptic specialization is a limiting factor in the development of compound activation in the developing ENS, pharmacologic activation and blockade of nicotinic neurotransmission were performed at EW14 and EW16, respectively. At EW14, application of 1 μmol/L acetylcholine led to significant contraction of fetal colonic tissue. This application did not result in compound activation of the presumptive ENS (Figure 5*D*, *E*, and *H* and Supplementary Movie 5). By contrast, application of high K$^+$ (300 mmol/L) led to stimulation of robust calcium transients in the presumptive ENS and contraction of the tissue (Figure 5*F*, *G*, and *H* and Supplementary Movie 5) (n = 2). Furthermore, by EW16, when electrical stimulation was found to elicit calcium transients in the ENS (Figure 5*I*, *J*, and *O* and Supplementary Movie 6), application of 300 μmol/L hexamethonium did not diminish such responses (Figure 5*K*, *L*, and *O* and Supplementary Movie 6, n = 1), whereas subsequent application of tetrodotoxin (TTX) (1 μmol/L) blocked compound activation of the fetal ENS (Figure 5*M*, *N*, and *O* and Supplementary Movie 6). Taken together, these results suggest that both synaptic and postsynaptic specialization are not rate-limiting factors in the development of stimulation-induced calcium activity in the early fetal ENS.

Transcriptional Changes in the Human Fetal Gut

To determine whether transcriptional changes might account for the apparent onset of electrical activity between EW14 and EW16, RNA sequencing analysis was performed across all developmental stages (EW12, EW14, and EW16) with stringent and more lenient read alignment procedures. Only minor differences between these procedures were observed (see Supplementary Materials sections "Lenient Alignment" and "Stringent Alignment"), allowing us to discriminate the expressions of different candidate gene homologues. With either one of these alignments, 13,828 genes were found to be expressed during EW12–EW16. Very low transcript levels were detected for 8,612 genes, making interpretation difficult, because such low levels may represent noise. For 30,828 genes, we were unable to detect any transcripts. With stage-specific analysis parameters (counts-per-million > 2 in specific embryonic week and <1 in the remaining 2), few of the detected genes were found to be specific for each of the time points included in this study (43 in EW12, 70 in EW14, and 80 in EW16). Many genes were also found to have different expression levels between EW12 and EW14 (n = 2265), between EW14 and EW16 (n = 3610), and between EW12 and EW16 (n = 3792). Most of these genes are known to affect many canonical pathways and biological functions, more than

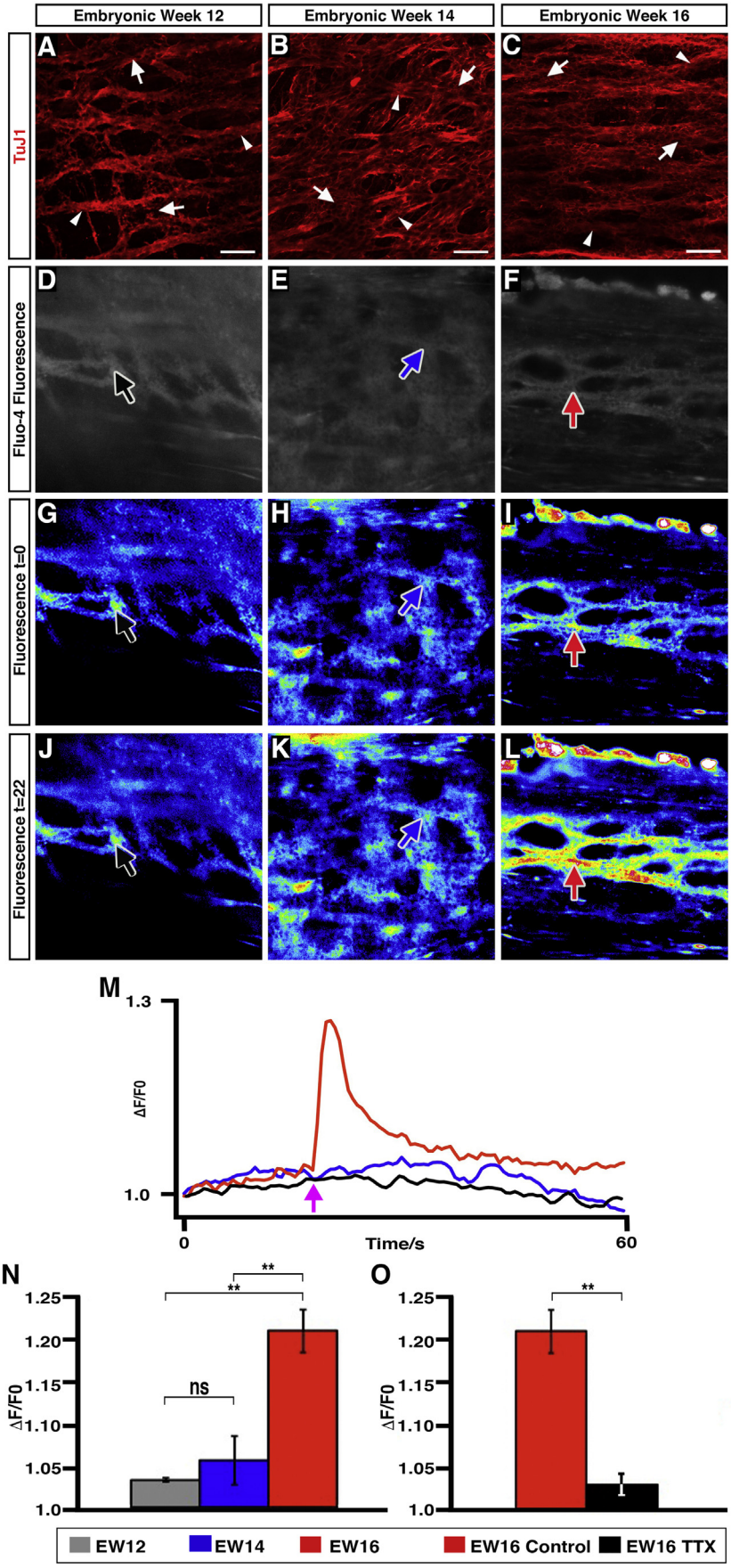

Figure 4. Induced calcium activity in the human fetal colon. (*A–C*) Representative confocal *z*-stacks of whole-mount colonic preparations. In (*A*) EW12, (*B*) EW14, and (*C*) EW16, whole-mount colonic preparations showed robust TuJ1$^+$ neural networks at the level of the myenteric plexus. In the myenteric plexus, TuJ1$^+$ neurons were observed in complex anastomosing networks with ganglia-like structures (*arrows*) and interganglionic neuronal connections (*arrowheads*). (*D–F*) Whole-mount preparations loaded with Fluo-4AM (Thermo Fisher Scientific, Waltham, MA) calcium indicator. (*G–I*) Representative pseudo-colored images at $t = 0$ seconds in (*G*) EW12, (*H*) EW14, and (*I*) EW16. (*J–L*) Representative pseudo-colored images at $t = 22$ seconds, after electrical stimulation, in (*G*) EW12, (*H*) EW14, and (*I*) EW16 preparations. Arrows represent regions of interest shown in representative traces below. (*M*) Representative traces of calcium activity in regions of interest indicated in *G–L*; magenta arrow represents time of stimulation. Note the absence of any induced calcium transient in EW12 and EW14 colonic preparations. In contrast, calcium transients were observed upon stimulation in EW16 preparations. (*N*) Summary data showing peak stimulation-induced calcium activity ($\Delta F/F_0$) in EW12 (*grey bar*, n = 3), EW14 (*blue bar*, n = 5), and EW16 (*red bar*, n = 3) colonic preparations. $^{**}P < .01$ by Tukey test. (*O*) Summary data showing peak stimulation-induced calcium activity ($\Delta F/F_0$) in EW16 colonic preparations in control conditions (*solid red bar*, n = 3) and after application of 1 μmol/L TTX (*hashed red bar*, n = 3). $^{**}P < .01$ by Student *t* test. ns, not significant.

expected by chance alone. Comparing EW12 to EW14 and EW16, we could see that, from a neuronal perspective, interesting characteristics and biological functions such as axogenesis, neuronal and synaptic development, quantity of neurons and neuronal tissue, sprouting, and ion transport were significantly enriched (negative *Z*-score). Moreover, we observed that expression of messenger RNA encoding proteins that may contribute to functions such as Ca^{2+} flux and cation, divalent cation, ionic, and Ca^{2+} mobilization, were significantly up-regulated (negative *Z*-score) compared with earlier time points (EW12–EW14) but were down-regulated (positive *Z*-score) at later stages

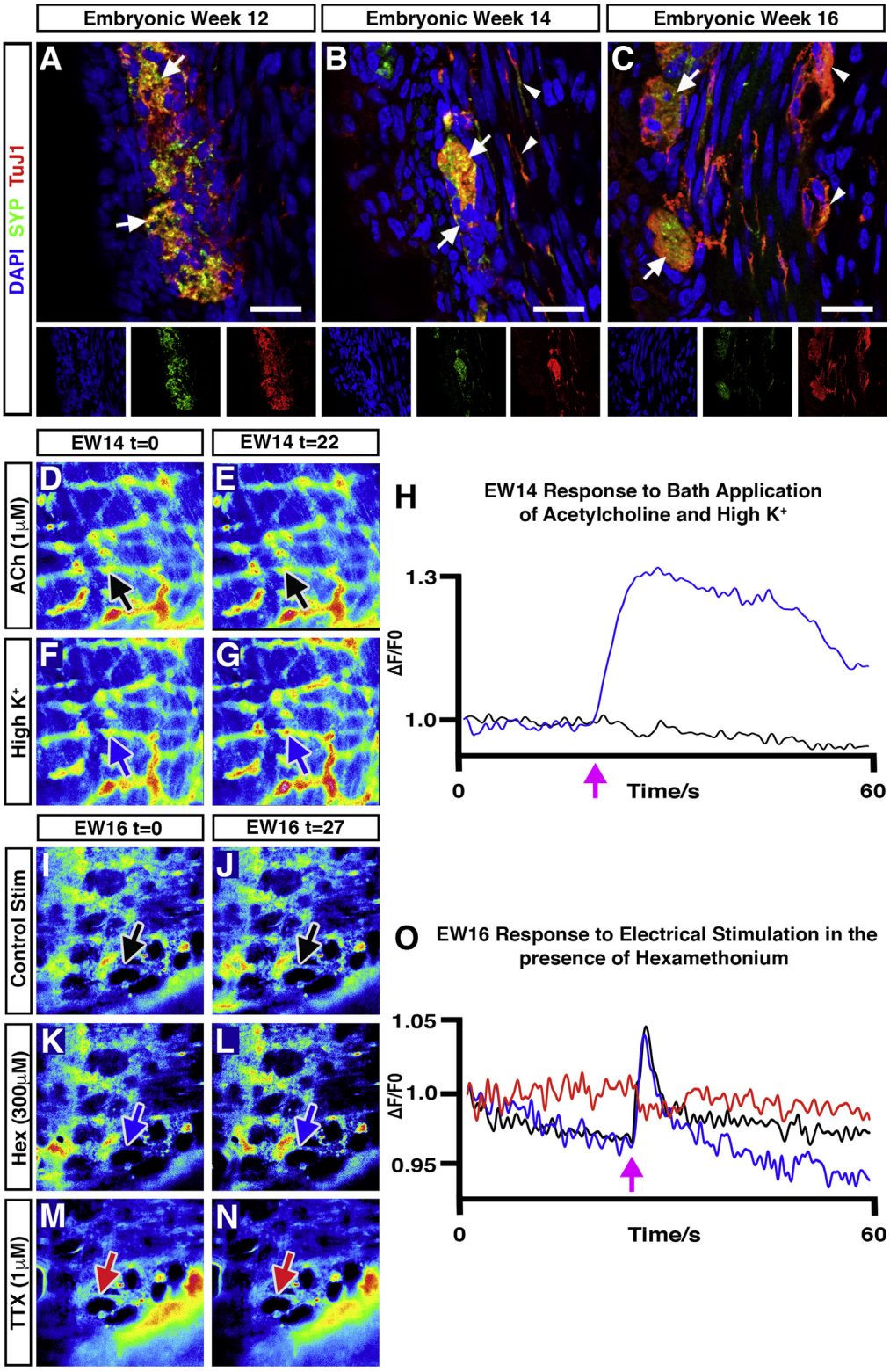

(EW14–EW16) (see Supplementary Materials section "Pathway Enrichment"). To validate these results, we specifically looked at the expression levels of 36 genes known to encode ion channels, neuronal subtypes, glial cells, synapsins, and semaphorins. We initially analyzed expression levels by plotting their counts-per-million values in a heatplot (Figure 6 and Supplementary Figure 5). This approach showed up-regulation of almost all of these genes in EW14 and EW16 colonic tissue compared with EW12. We also performed qRT-PCR analysis on 3 independent colonic samples from each developmental stage (EW12–EW16). The results obtained showed an up-regulation of the expression levels of candidate Na^+ (SCN) and K^+ (KNCQ) channel–expressing genes known to be involved in the generation and modulation of ENS action potentials. Each candidate ion channel examined (*SCN2A*, *SCN3A*, *SCN5A*, *SCN8A*, *SCN9A*, *KCNQ2*, and *KCNQ3*) displayed a trend toward increased expression between EW12 and EW16 (Figure 7*A* and Supplementary Table 4). *SCN3A*, which encodes a TTX-sensitive, fast-inactivating, voltage-gated Na^+ channel and plays a major role in neuronal action potentials, displayed a linear increasing trend in expression, with a 1.10-fold increase at EW14 and a 1.44-fold increase at EW16, compared with EW12 colonic tissue. Similarly, *SCN9A*, which has been shown to modify neuron excitability during the relative refractory period, displayed a linear increasing trend in expression, with a 1.51-fold increase at EW14 and a 2.13-fold increase at EW16, compared with EW12 colonic tissue. In contrast, other candidate genes, *KCNQ2* and *KCNQ3*, which encode delayed rectifier K^+ channels and act to regulate membrane excitability and the threshold for action potential generation, displayed increases in expression between EW12 and EW14, with subsequent reduction in expression at EW16. Up-regulation of these ion channels might account for evoked activity at EW16. Concerning the expression levels of several ENS candidate genes, the expression patterns observed in terms of neuronal subtypes corresponded to the temporal development pattern observed in immunohistochemical analysis. VAChT expression was maintained at a relatively constant level across the 3 developmental time points (Figure 7*B* and Supplementary Table 4), whereas nNOS expression displayed an increase at EW14, which corresponds to the birthdating of this neuronal subtype. Expression of both *TAC-1*, a precursor of Sub P, and *VIP* also mimicked immunohistochemical observations, with increasing expression up to EW16. *S100* expression increased at EW14, which appears to match a possible transitional and transient period of $S100^+$ glial cell development, as visualized by immunofluorescence. *SYN1* expression remained relatively constant across each time point, supporting our earlier findings that synaptic proteins are already expressed by EW12. Finally, *SEMA3A*, a gut morphogen previously found to affect ENS development, showed a modest increase in expression between EW12 and EW14, which appeared to plateau at EW16. Taken together, these data suggest that rather than a significant shift in expression of a single ion channel or ion channel family, a trend in increasing expression of a range of critical ion channels appears to account for the changes in ENS neurotransmission across this 4-week period. These data also confirm our immunohistochemical findings, further supporting the idea that the developmental time window between EW12 and EW16 is critical for the establishment of a repertoire of neuronal subtypes and enteric glia.

Discussion

Extensive murine studies with immunohistochemical analysis and various reporter mice have established the temporal development pattern of the enteric nervous system (ENS), including the onset of spontaneous and induced electrical activity in embryonic mouse gut.[4,8–11,17–25] However, such knowledge about the developing human gut is lacking. In this study, we report that the onset of evoked electrical activity in the human fetal ENS appears at approximately EW16. We show that such activity appears to coincide with increases in gene expression of various ion channels known to modulate enteric action potentials, and we clearly establish the temporal development of a number of neural subtypes and enteric glia between EW12 and EW16. Furthermore, we confirm such temporal development with gene expression studies that highlight the developmental processes required for the establishment of a functional ENS.

In this study, the proximal colon was chosen as a site of investigation for both technical and translational purposes. The identification of the caecum in intestinal specimens, across developmental time points, critically allowed for characterization of an anatomically consistent region

Figure 5. Synaptic protein expression and functional postsynaptic specialization in the human fetal colon. (*A–C*) Representative high-power immunofluorescent images of colonic cryosections at (*A*) EW12, (*B*) EW14, and (*C*) EW16 showing the expression of TuJ1 (*red*), synaptophysin (SYP, *green*), and DAPI (*blue*). (*A*) At EW12, coexpression of TuJ1 and synaptophysin was observed in ganglia-like structures of the myenteric plexus (*arrows*). (*B*, *C*) At EW14 and EW16 coexpression of TuJ1 and synaptophysin was observed in the myenteric plexus region (*arrows*) and in the submuscosal region (*arrowheads*). Scale bars, 50 μm. (*D–H*) Representative activity of EW14 fetal colonic tissue in the presence of acetylcholine (1 μmol/L) and high K^+. (*D*, *E*) Pseudo-colored images of calcium activity in the presumptive ENS at (*D*) $t = 0$ seconds and (*E*) $t = 22$ seconds, after application of acetylcholine (1 μmol/L). (*F*, *G*) Pseudo-colored images of calcium activity at (*F*) $t = 0$ seconds and (*G*) $t = 22$ seconds, after application of high K^+. Arrows represent regions of interest shown in representative traces shown in *H*. (*H*) Representative traces of calcium activity in regions of interest are indicated in *D–G*; magenta arrow represents time of pharmacologic application. (*I–N*) Representative pseudo-colored images of calcium activity in the ENS at $t = 0$ seconds and, after electrical stimulation, at $t = 27$ seconds in control conditions (Krebs; *I*, *J*), in the presence of hexamethonium (300 μmol/L; *K*, *L*) and after the application of TTX (1 μmol/L; *M*, *N*). Arrows represent regions of interest shown in representative traces shown in *O*. (*O*) Representative traces of calcium activity in regions of interest indicated in *I–N*; magenta arrow represents time of electrical stimulation. DAPI, 4′,6-diamidino-2-phenylindole.

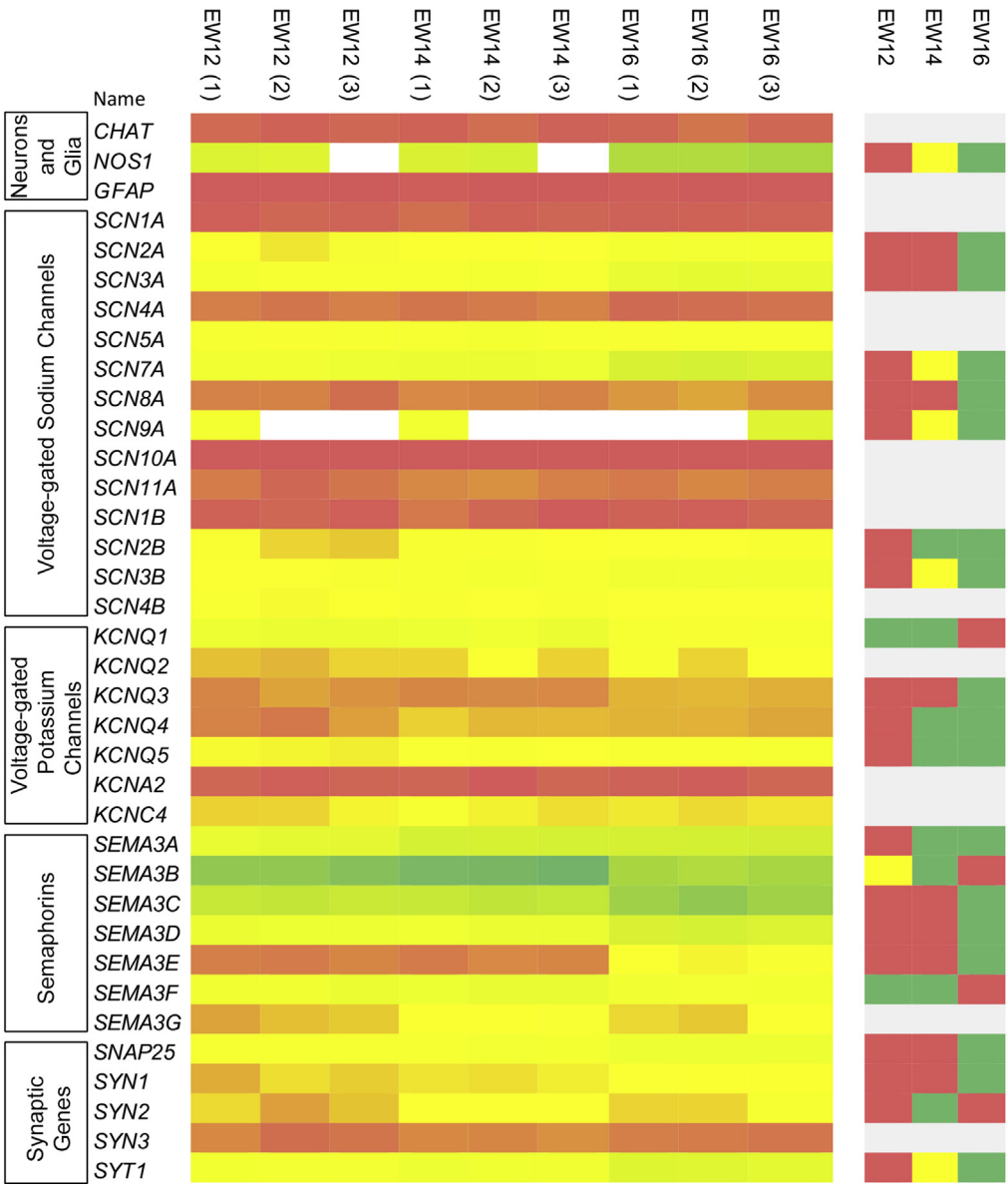

Figure 6. Representative gene expression heatplot for candidate genes in the human fetal colon. Heatplot based on RNA sequencing analysis (lenient analysis parameters) (*left*) of individual fetal colon samples, showing gene expression (*left*) at EW12, EW14, and EW16 (low relative expression [*red*] and high relative expression [*green*]). Average expression by time point (*right*) shows directionality of expression from lower expression (*red*) to higher expression (*green*). Significant changes in gene expression represent false discovery rate values ≤ 0.05.

(proximal colon) in all specimens. Moreover, the most common congenital gut motility defects, including Hirschsprung disease and slow transit constipation, are known to affect the colonic region.[26] Therefore, a better understanding of the normal ENS developmental timeline, in this region, may provide a means of understanding factors and disease processes that influence functional development.

The formation of circuitry and the development of coordinated electrical activity are crucial requirements for normal bowel function. Disruptions in neuronal plexus formation, density, or diversity severely affect physiological output.[19,27–31] In showing the development of several key enteric neuronal subtypes from EW12 to EW14 and the subsequent development of coordinated electrical activity at EW16, we believe that this 4-week developmental time period is critical for the correct assembly of a functional ENS. Of note, the current study examined the development of evoked activity in the proximal colon and, as such, the findings presented may not be reflective of the functional development of other gut segments. Recent studies in animal models have highlighted that routinely available pharmacologic agents such as ibuprofen or vitamin A deficiency can affect ENS development.[32,33] Hence, it is conceivable that in this critical developmental window in the early second trimester, the ENS is vulnerable to insult, which may be clinically relevant in terms of subtle disease processes.

Our findings from both RNA-sequencing and qRT-PCR analyses suggest a general up-regulation of a number of ion channels and increasing diversity of enteric neurons and glia over this period. The methodology used in the current study involved whole-tissue segments rather than direct isolation of native ENCCs. As such, the inclusion of non-ENCCs may have diluted the expression of specific ENCC-related genes and may account for the failure of our

comparison analysis to reach statistical significance. A previous murine study showed a similar general up-regulation of ion channel expression between E11.5 and E14.5.[34] This study made use of endogenous yellow fluorescent protein (YFP) expression in murine ENCCs to enable specific isolation of ENCCs at each time point via fluorescence activated cell sorting. Although previous studies have successfully isolated small numbers of ENCCs from human fetal tissue[15,35] using p75 fluorescence-activated cell sorting isolation, the limited availability of fetal human gut samples and the need for physiological and immunohistochemical analyses in the current study prevented the specific isolation of sufficient numbers of ENCCs. Furthermore, 1 embryo per time point was examined for this initial analysis, and the groups presented in the differential expression analysis represent technical replicates. Therefore, our differential expression analysis should be viewed as an indicator of the transcriptional difference between the developmental stages examined.

In this study, we clearly show that coordinated compound activation of enteric networks occurs between EW14 and EW16, showing a critical period of gut development that may underpin functionality in later life. The finding that 4 of 5 human colon samples at EW14 did not display electrical activity, compared with 3 of 3 at EW16 that did display Ca^{2+} transients upon electrical stimulation, suggests that this window of activation is consistent across numerous fetal gut specimens. Similarly, immunohistochemical analysis of the temporal development of neural subtypes and glia was found to be consistent across multiple specimens. The staging method used in this study relies on measurement of either knee-to-heel length or foot length. Although this method has been validated, the resolution of gestational age in weeks may lead to minor discrepancies in precise staging. It is therefore likely that the sample (1 of 5) that displayed electrical activity at EW14 in response to stimulation may represent late-stage EW14/EW15 tissue. Spontaneous Ca^{2+} oscillations were not resolved in the human ENS specimens examined. Previous investigations in murine gut samples suggest that spontaneous calcium transients occur from E11.5 to E15.5, which can propagate to neighboring ENCCs. This spontaneous calcium activity appeared to be a transient phenomenon, as such activity was not observed in either E10.5 or E16.5 tissue.[10] Given that this transient activity in mice commences before full colonization of the gut and then ceases shortly after ENCCs have completed their rostrocaudal migration along the length of the gut, it is likely that spontaneous calcium activity was not observed in human specimens because of the timeframe of our current study, because complete colonization of the human gut has been shown to occur by approximately EW7.

The finding that inhibitory neuronal subtypes in the colon, including nNOS and VIP, appear to arise at approximately EW14 after excitatory neuronal subtypes (VAChT

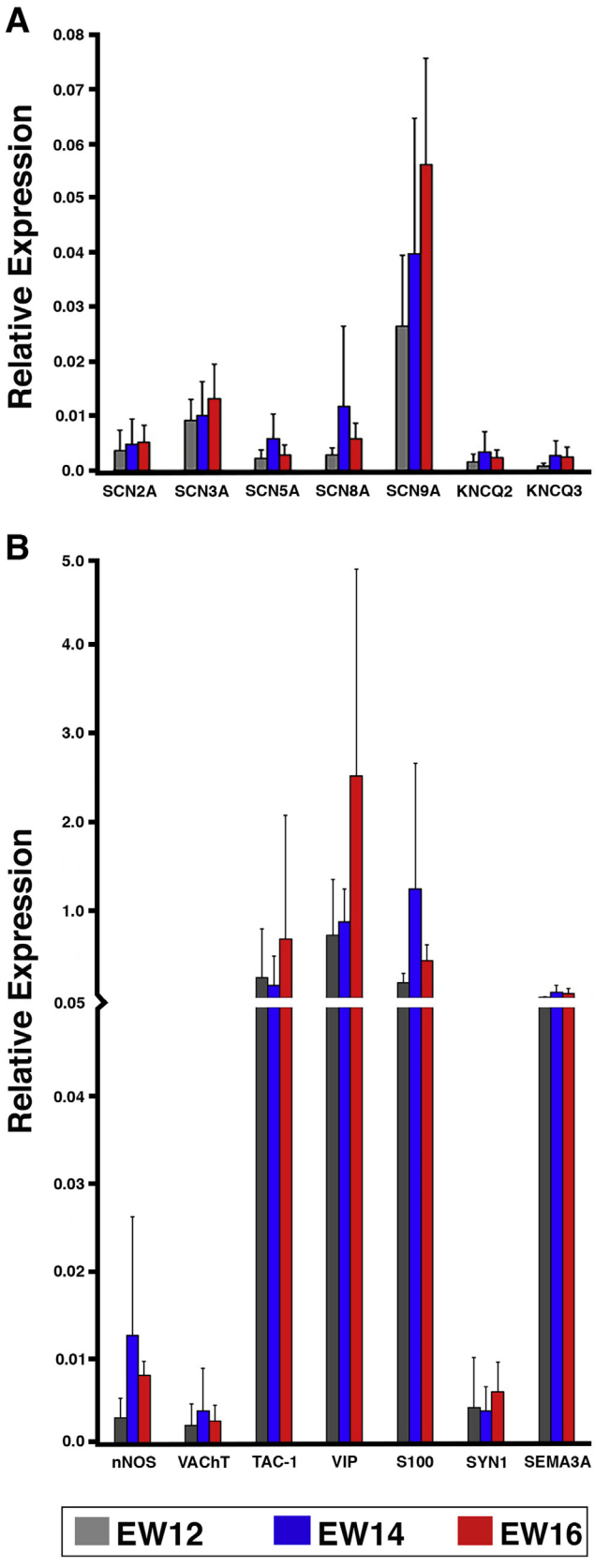

Figure 7. qRT-PCR analysis of candidate gene expression in the human fetal colon. (*A*) Quantification of candidate ion channel gene expression in EW12 (*grey bars*), EW14 (*blue bars*), and EW16 (*red bars*). (*B*) Quantification of candidate gene expression for markers for enteric neurons and glia in EW12 (*grey bars*), EW14 (*blue bars*), and EW16 (*red bars*).

and Sub P) suggests that there is an extended period of neuronal modulation after ENCC colonization. In murine studies, $ChAT^+$ neurons were found to develop in the colon from E14.5,[10] whereas $nNOS^+$ neurons have previously been shown to arise between E12.5[8] and E13.5 (E11.5 + 48-hour culture).[18] The reasons behind the contrasting findings in terms of neuronal birth-dating are unclear. Unfortunately, in our hands, various immunohistologic assays with ChAT antibodies in human gut tissue proved unsuccessful. However, complexities in the transcriptional and post-transcriptional regulation of ChAT and VAChT may account for the different timings observed in the 2 species.[36] Our finding that synaptic proteins are expressed at EW12, several weeks before the onset of coordinated activity, suggests that although physical expression of synaptic proteins exists in the human ENS by the end of the first trimester, further modulation and refinement of the mechanisms involved in neuronal excitability occurs in the following weeks to allow coordinated, networked activity by EW16. We show that acetylcholine stimulation, at EW14 did not elicit compound activation of the presumptive ENS and that blockade of nicotinic acetylcholine receptors at EW16 did not block stimulation-induced Ca^{2+} transients in the fetal ENS. This suggests that both synaptic and postsynaptic nicotinic specializations are not critical factors in the development of evoked calcium activity in the early human ENS.

Previous studies have suggested that neural activity may act to influence ENS wiring.[17,18] During mouse development, neurons transition from inactive to action potential firing with increasing voltage-gated sodium channel expression and increasing Na^+ current density.[17] All embryonic action potentials in murine neurons in that study appeared to be TTX sensitive. Similarly, in our current study, coordinated firing of enteric neural networks upon stimulation at EW16 were TTX sensitive. Taken together, these results suggest that a similar developmental pattern may be responsible for action potential firing in early human fetal gut. The requirement for coordinated firing of the human ENS relatively early in gestation remains unclear. Although there is accumulation of meconium in the fetal human gut at the early stages, fully developed motor patterns are not established until well into postnatal development.[37–39] Therefore, further studies will be required to establish how the development of ENS activity in the human gut influences not only neural development per se but also the impact on associated cell types in the neuromuscular syncytium that ultimately dictate motility.

We conclude that this study provides critical evidence describing the birth-dating of neuronal subtypes and the subsequent emergence of coordinated electrical activity in the human ENS and thus may provide a platform for future studies to understand the developmental and pathophysiological basis of enteric neuropathies in the human gastrointestinal tract.

Data Availability

The data that support the findings of this study are available from the corresponding author upon reasonable request. Transcript profiling: RNA sequencing data are deposited in the Gene Expression Omnibus database (https://www.ncbi.nlm.nih.gov/geo/) under the accession number GSE111307.

Supplementary Material

Note: To access the supplementary material accompanying this article, visit the online version of *Gastroenterology* at www.gastrojournal.org, and at https://doi.org/10.1053/j.gastro.2018.12.020.

References

1. Furness JB. The enteric nervous system. Malden, MA: Blackwell, 2006.
2. Burns AJ, Douarin NM. The sacral neural crest contributes neurons and glia to the post-umbilical gut: spatiotemporal analysis of the development of the enteric nervous system. Development 1998;125:4335–4347.
3. Kapur RP, Yost C, Palmiter RD. A transgenic model for studying development of the enteric nervous system in normal and aganglionic mice. Development 1992; 116:167–175.
4. Young HM, Hearn CJ, Ciampoli D, et al. A single rostrocaudal colonization of the rodent intestine by enteric neuron precursors is revealed by the expression of Phox2b, Ret, and p75 and by explants grown under the kidney capsule or in organ culture. Dev Biol 1998;202:67–84.
5. Wang X, Chan AK, Sham MH, et al. Analysis of the sacral neural crest cell contribution to the hindgut enteric nervous system in the mouse embryo. Gastroenterology 2011;141:992–1002.
6. Nishiyama C, Uesaka T, Manabe T, et al. Trans-mesenteric neural crest cells are the principal source of the colonic enteric nervous system. Nat Neurosci 2012; 15:1211–1218.
7. Lasrado R, Boesmans W, Kleinjung J, et al. Lineage-dependent spatial and functional organization of the mammalian enteric nervous system. Science 2017; 356:722–726.
8. Young HM, Jones BR, McKeown SJ. The projections of early enteric neurons are influenced by the direction of neural crest cell migration. J Neurosci 2002;22:6005–6018.
9. Hao MM, Bornstein JC, Young HM. Development of myenteric cholinergic neurons in ChAT-Cre;R26R-YFP mice. J Comp Neurol 2013;521:3358–3370.
10. Hao MM, Bergner AJ, Hirst CS, et al. Spontaneous calcium waves in the developing enteric nervous system. Dev Biol 2017;428:74–87.
11. Hao MM, Boesmans W, Van den Abbeel V, et al. Early emergence of neural activity in the developing mouse enteric nervous system. J Neurosci 2011; 31:15352–15361.
12. Fu M, Tam PK, Sham MH, et al. Embryonic development of the ganglion plexuses and the concentric layer structure of human gut: a topographical study. Anat Embryol (Berl) 2004;208:33–41.
13. Wallace AS, Burns AJ. Development of the enteric nervous system, smooth muscle and interstitial cells of Cajal in the human gastrointestinal tract. Cell Tissue Res 2005; 319:367–382.

14. Cooper JE, McCann CJ, Natarajan D, et al. In vivo transplantation of enteric neural crest cells into mouse gut; engraftment, functional integration and long-term safety. PLoS One 2016;11:e0147989.
15. Cooper JE, Natarajan D, McCann CJ, et al. In vivo transplantation of fetal human gut-derived enteric neural crest cells. Neurogastroenterol Motil 2017;29:e12900.
16. Halim D, Wilson MP, Oliver D, et al. Loss of LMOD1 impairs smooth muscle cytocontractility and causes megacystis microcolon intestinal hypoperistalsis syndrome in humans and mice. Proc Natl Acad Sci U S A 2017;114:E2739–E2747.
17. Hao MM, Lomax AE, McKeown SJ, et al. Early development of electrical excitability in the mouse enteric nervous system. J Neurosci 2012;32:10949–10960.
18. Hao MM, Moore RE, Roberts RR, et al. The role of neural activity in the migration and differentiation of enteric neuron precursors. Neurogastroenterol Motil 2010; 22:e127–e137.
19. Sasselli V, Boesmans W, Vanden Berghe P, et al. Planar cell polarity genes control the connectivity of enteric neurons. J Clin Invest 2013;123:1763–1772.
20. Young HM, Bergner AJ, Anderson RB, et al. Dynamics of neural crest-derived cell migration in the embryonic mouse gut. Dev Biol 2004;270:455–473.
21. Foong JP, Hirst CS, Hao MM, et al. Changes in nicotinic neurotransmission during enteric nervous system development. J Neurosci 2015;35:7106–7115.
22. Foong JP, Nguyen TV, Furness JB, et al. Myenteric neurons of the mouse small intestine undergo significant electrophysiological and morphological changes during postnatal development. J Physiol 2012;590:2375–2390.
23. Foong JP, Tough IR, Cox HM, et al. Properties of cholinergic and non-cholinergic submucosal neurons along the mouse colon. J Physiol 2014;592:777–793.
24. Fung C, Boesmans W, Cirillo C, et al. VPAC receptor subtypes tune purinergic neuron-to-glia communication in the murine submucosal plexus. Front Cell Neurosci 2017;11:118.
25. Koussoulas K, Swaminathan M, Fung C, et al. Neurally released GABA acts via GABAC receptors to modulate Ca(2+) transients evoked by trains of synaptic inputs, but not responses evoked by single stimuli, in myenteric neurons of mouse ileum. Front Physiol 2018;9:97.
26. Pesce M, Borrelli O, Saliakellis E, et al. Gastrointestinal neuropathies: new insights and emerging therapies. Gastroenterol Clin North Am 2018;47:877–894.
27. Kapoor A, Auer DR, Lee D, et al. Testing the Ret and Sema3d genetic interaction in mouse enteric nervous system development. Hum Mol Genet 2017; 26:1811–1820.
28. McCann CJ, Cooper JE, Natarajan D, et al. Transplantation of enteric nervous system stem cells rescues nitric oxide synthase deficient mouse colon. Nat Commun 2017;8:15937.
29. Uesaka T, Enomoto H. Neural precursor death is central to the pathogenesis of intestinal aganglionosis in Ret hypomorphic mice. J Neurosci 2010;30:5211–5218.
30. Brun P, Giron MC, Qesari M, et al. Toll-like receptor 2 regulates intestinal inflammation by controlling integrity of the enteric nervous system. Gastroenterology 2013; 145:1323–1333.
31. Anitha M, Gondha C, Sutliff R, et al. GDNF rescues hyperglycemia-induced diabetic enteric neuropathy through activation of the PI3K/Akt pathway. J Clin Invest 2006;116:344–356.
32. Fu M, Sato Y, Lyons-Warren A, et al. Vitamin A facilitates enteric nervous system precursor migration by reducing Pten accumulation. Development 2010;137:631–640.
33. Schill EM, Lake JI, Tusheva OA, et al. Ibuprofen slows migration and inhibits bowel colonization by enteric nervous system precursors in zebrafish, chick and mouse. Dev Biol 2016;409:473–488.
34. Hirst CS, Foong JP, Stamp LA, et al. Ion channel expression in the developing enteric nervous system. PLoS One 2015;10:e0123436.
35. Metzger M, Caldwell C, Barlow AJ, et al. Enteric nervous system stem cells derived from human gut mucosa for the treatment of aganglionic gut disorders. Gastroenterology 2009;136:2214–2225.
36. Castell X, Diebler MF, Tomasi M, et al. More than one way to toy with ChAT and VAChT. J Physiol Paris 2002; 96:61–72.
37. Bisset WM, Watt JB, Rivers RP, et al. Measurement of small-intestinal motor activity in the preterm infant. J Biomed Eng 1988;10:155–158.
38. Baker J, Berseth CL. Postnatal change in inhibitory regulation of intestinal motor activity in human and canine neonates. Pediatr Res 1995;38:133–139.
39. Amarnath RP, Berseth CL, Malagelada J-R, et al. Postnatal maturation of small intestinal motility in preterm and term infants. Neurogastroenterol Motil 1989;1: 138–143.

Received April 29, 2018. Accepted December 24, 2018.

Reprint requests
Address requests for reprints to: Nikhil Thapar, MD, PhD, Stem Cells and Regenerative Medicine, UCL Great Ormond Street Institute of Child Health, 30 Guilford Street, London, WC1N 1EH, UK. e-mail: n.thapar@ucl.ac.uk; fax: +44 2079052953.

Acknowledgments
The human embryonic and fetal material was provided by the Joint MRC/Wellcome Trust grant no. 099175/Z/12/Z Human Developmental Biology Resource (http://hdbr.org). The authors would like to acknowledge the NIHR Great Ormond Street Hospital Biomedical Research Centre, which supports all research at Great Ormond Street Hospital NHS Foundation Trust and UCL Great Ormond Street Institute of Child Health. The views expressed are those of the author(s) and not necessarily those of the NHS, the NIHR, or the Department of Health. The authors acknowledge the support of Prince Abdullah Ben Khalid Celiac Research Chair, College of Medicine, Vice-Deanship of the Research Chairs, King Saud University, Riyadh, Saudi Arabia.

Author contributions: Conor J. McCann, Maria M. Alves, Erwin Brosens, Dipa Natarajan, Silvia Perin, and Chey Chapman acquired and interpreted data. Robert M. W. Hofstra, Alan J. Burns, and Nikhil Thapar interpreted data and obtained funding. Conor J. McCann, Robert M. W. Hofstra, Alan J. Burns, and Nikhil Thapar contributed to study concept and design and drafted the manuscript.

Conflicts of interest
The authors disclose no conflicts.

Funding
Nikhil Thapar is supported by Great Ormond Street Hospital Children's Charity (GOSHCC; V1258). This work was funded through a GOSHCC grant (W1018C) awarded to Nikhil Thapar (principal investigator) and Alan J. Burns (coinvestigator). Conor J. McCann is supported by Guts UK (Derek Butler Fellowship).

Supplementary Materials and Methods

Immunohistochemistry

Whole-mount immunohistochemistry was performed on fetal colonic segments after excision and removal of the mucosa by sharp dissection. Tissues were fixed in paraformaldehyde (4% weight/volume in 0.1 mol/L phosphate buffered saline (PBS) for 45 minutes at 22°C), washed for 24 hours in PBS (0.01 mol/L, pH 7.2 at 4°C), blocked for 1 hour (0.1 mol/L PBS containing 1% Triton X-100, 1% bovine serum albumin [BSA]), and incubated in primary antibody (diluted in 0.1 mol/L PBS containing 1% Triton X-100, 1% BSA) (Supplementary Table 1) for 48 hours at 4°C. Immunoreactivity was detected with the secondary antibodies listed in Supplementary Table 2 (1:500 in 0.1 mol/L PBS, 1 hour at room temperature). Before mounting, tissues were washed thoroughly in PBS (0.1 mol/L PBS for 2 hours at 22 °C).

For cryostat sections, colonic tissues were fixed in paraformaldehyde (4% weight/volume in 0.1 mol/L PBS for 45 minutes at 22°C) after excision, washed for 24 hours in PBS (0.01 mol/L, pH 7.2 at 4°C), cryoprotected in 0.1 mol/L PBS containing 30% sucrose (24 hours at 4°C), and embedded in gelatin (7.5% weight/volume in 0.1 mol/L PBS containing 15% sucrose). Subsequently, tissues were frozen at –65°C in isopentane and stored at –80°C. Frozen, embedded samples were sectioned serially (20 μm) with a Cam 1900 UV Cryostat (Leica Microsystems, Milton Keynes, UK), and slides were stored at –20°C for further processing.

For cryosection immunohistochemistry, slides were thawed and heated to 37°C in 0.01 mol/L PBS for 20 minutes to remove excess gelatin. Tissues were postfixed in paraformaldehyde (4% weight/volume in 0.1 mol/L PBS for 10 minutes at 22°C), washed 3 × 20 minutes in PBS (0.01 mol/L, pH 7.2 at 4°C), blocked for 1 hour (0.1 mol/L PBS containing 1% Triton X-100, 1% BSA). Tissues were incubated in primary and secondary antibodies, as described. Before mounting, sections were washed thoroughly in PBS (0.1 mol/L PBS 3 × 20 minutes at 22°C). Control tissues were prepared by omitting primary or secondary antibodies.

Tissues and sections were examined with a LSM710 Meta confocal microscope (Carl Zeiss, Oberkochen, Germany). Whole-mount confocal micrographs were digital composites of the Z-series of scans (0.5-μm optical sections), and confocal micrographs of cryostat sections were single plane images. Final images were constructed using FIJI software.[35]

Calcium Imaging

Fetal intestinal samples were obtained as previously described, and calcium imaging was performed as previously reported.[29] Briefly, tissues were immersed in previously oxygenated (95% oxygen/5% carbon dioxide) Krebs solution (in mmol/L: 120.9 NaCl, 5.9 KCl, 1.2 $MgCl_2$, 2.5 $CaCl_2$, 11.5 glucose, 14.4 $NaHCO_3$, and 1.2 NaH_2PO_4). After excision of the colon and removal of the mucosa by sharp dissection, tissue samples were flipped serosal side up, and strips of the longitudinal muscle were removed by sharp dissection to show the underlying myenteric plexus. Colonic preparations were pinned tightly, serosal side up, in a Sylgard-lined chamber. Tissues were then loaded with the fluorescent Ca^{2+} indicator Fluo-4AM (5 μmol/L) (Thermo Fisher Scientific, Waltham, MA) and Cremophor EL (0.00001%) (Fluka Chemika, Buchs, Switzerland) in Krebs solution at room temperature for 20 minutes with continuous oxygenation. After loading, tissues were washed (2 × 10 minutes, Krebs) before imaging. Subsequently, the myenteric plexus was identified, and live fluorescence imaging was performed on an Olympus BX51 microscope equipped with a 20× water dipping lens (XLUMPlanFL N, NA 1; Olympus Europa; Hamburg, Germany), and an EMCCD camera (iXon Ultra 897; Andor Technology, Belfast, UK). Fluo-4 was excited at 470 nm using an OptoLED (Cairn Research Limited, Faversham, UK), and fluorescence emission was collected at 525/50 nm. Images (512 × 512 pixels^2) were acquired at 2 Hz. Electrical train stimulation (2 seconds, 20 Hz of 300-μs electrical pulses) (Electronic stimulator 1001, ADInstruments) was applied via a platinum/iridium electrode (tip diameter, 2–4 μm) (World Precision Instruments, Sarasota, FL) placed directly onto internodal strands in the presumptive myenteric plexus at a distance of 200 μm from the center of the field of view. Electrical point stimulation was applied as described, and images were collected with OptoFluor software (Cairn Research Limited, Faversham, UK). Postacquisition analysis was performed in Fiji.[35] Movement artefacts were removed by registering the image stack to the first image using the StackRef plugin.[36] Regions of interest (ROIs) of approximately 25 μm^2 were drawn on ganglia-like structures or interganglionic strands in the presumptive myenteric plexus. Subsequently, fluorescence intensity was normalized to basal fluorescence for each ROI ($\Delta F/F_0$), and peaks were analyzed. To evaluate statistical differences between groups, 5 ROIs, chosen at random from across the presumptive myenteric plexus, were analyzed from each individual fetal colon sample. Final images were constructed using Fiji software.[35]

RNA Sequencing Analysis

CLC-Bio (Qiagen, Venlo, The Netherlands) was used for subsequent quality control assessment, read trimming, alignment to the National Center for Biotechnology Information version 37 *Homo sapiens* reference genome, transcript quantification, and differential expression analysis. Reads were aligned by using the following settings: mismatch cost 2, insertion/deletion cost 3, length fraction 0.8, similarity fraction 0.8, alignment to gene regions only. Paired reads were counted as 1. Trimmed mean of *M* values[38,39] was used to normalize for sequencing depth across samples. Counts per million (CPM) values were calculated for each gene, centered, and scaled to unit variance. Expression values were counted as total counts and reads per kilobase of exon model per million mapped reads (RPKM).[40] RPKM values were used for sample gene

expression comparison and pathway enrichment analysis. Differential expression was calculated between groups, with the individual replicates per time point as a group. The CLC bio (Aarhus, Denmark) generalized linear model and Wald test were used as statistical models to test between groups.

Candidate Gene Expression Evaluation

Two types of output were generated: one in which reads were allowed to map to more than one location (lenient analysis) and another in which we allowed only uniquely mapped reads (stringent analysis). Lenient analysis was used for differential analysis, and stringent alignment was used to validate the specificity of the expression of paralogous genes of interest (sodium voltage-gated channel α subunits, sodium channel epithelial β subunits, synapsins, and semaphorins). When evaluating expression, we considered a gene to be *expressed* if it had an average CPM value of ≥ 2 for all genes across triplicates, *uncertain* when CPM values were between 1 and 2, and *not expressed* if the average CPM value was <1. If embryologic stages differed significantly (FDR $\leq$ 0.05), we considered the direction of the change to be true if not we could not determine the directionality of the change with RNA sequencing. Raw data and the output of the lenient and stringent alignments, including CPM, total counts, RKPM, TPM, and statistics, are available at the Gene Expression Omnibus database (https://www.ncbi.nlm.nih.gov/geo/), under the accession number GSE111307.

Causal Network Analysis Using Ingenuity Pathway Analysis

Differently expressed genes (false discovery rate $\leq$ 0.05) with a fold change $\geq$ 1.5 and a RPKM group mean >1 were uploaded to Ingenuity Pathway Analysis (Qiagen) for downstream pathway analysis. The causal networks analysis algorithm embedded in the Ingenuity Pathway Analysis tool was used to infer cause-effect relationships from the gene expression data results.[41] As thresholds for significance, we used a P value $\leq$ .05 and a Z-score of 2.

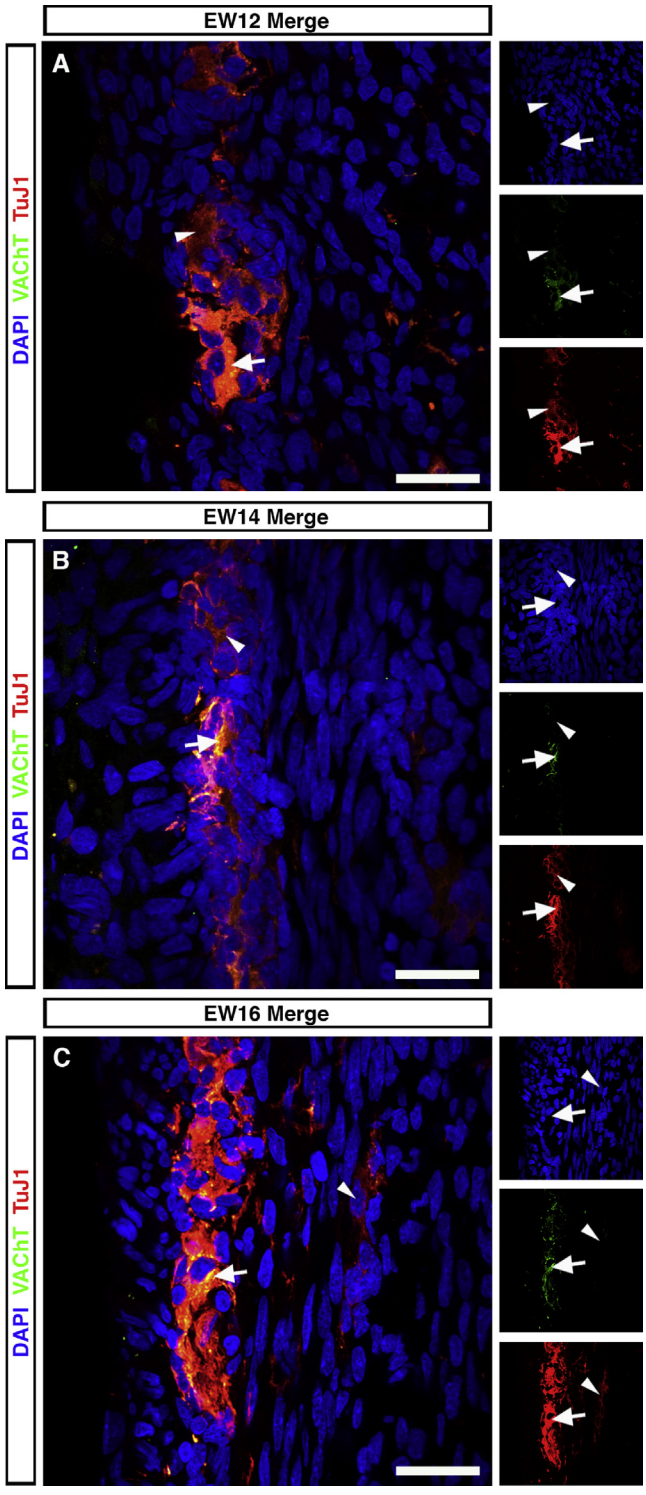

Supplementary Figure 1. Development of VAChT^{+} neurons in the human fetal colon. (*A–C*) Representative high-power immunofluorescent images showing expression of TuJ1 (*red*), VAChT (*green*), and DAPI (*blue*) in the developing fetal colon. At (*A*) EW12, (*B*) EW14, and (*C*) EW16, coexpression of TuJ1 and VAChT was observed in numerous cells at the level of the myenteric plexus (*arrows*). In addition, TuJ1^{+} cells not expressing VAChT were observed (*arrowheads*). Scale bars, 25 μm. DAPI, 4′,6-diamidino-2-phenylindole.

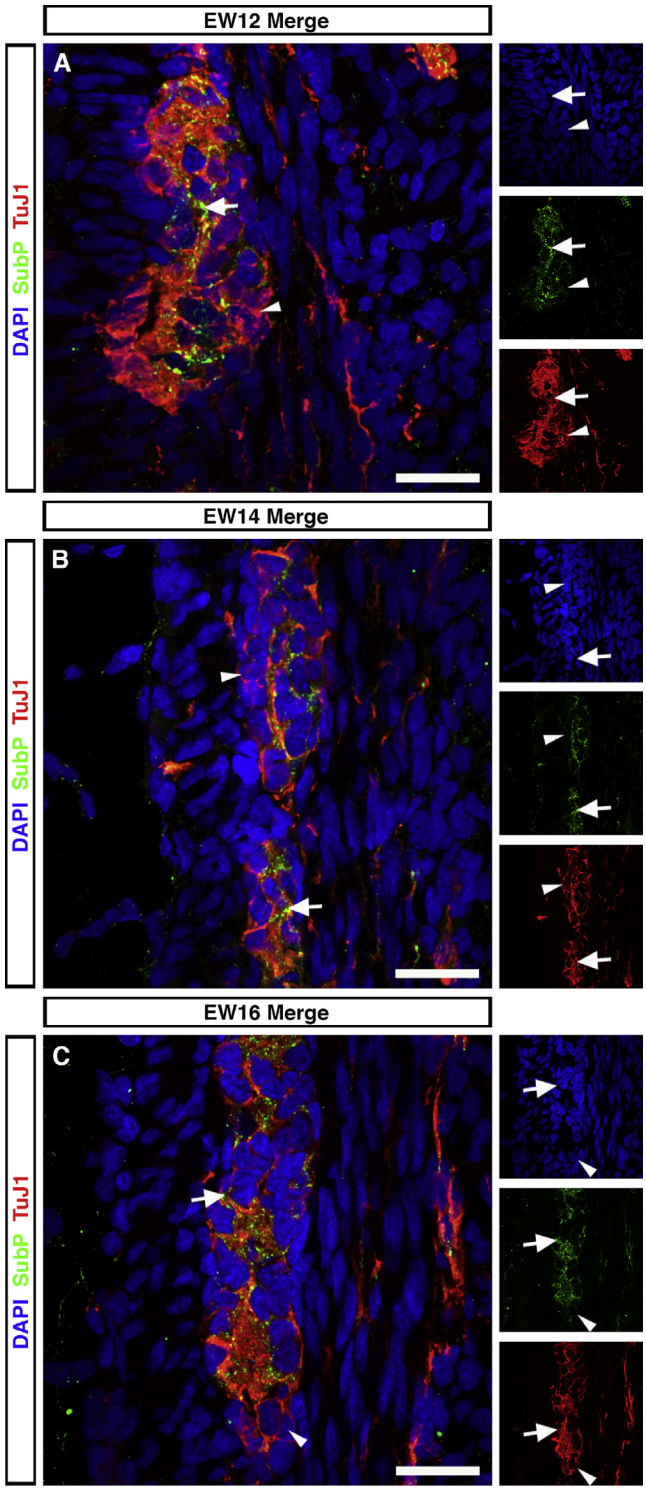

Supplementary Figure 2. Development of Sub P^{+} neurons in the human fetal colon. (*A–C*) Representative high-power immunofluorescent images showing expression of TuJ1 (*red*), Sub P (*green*), and DAPI (*blue*) in the developing fetal colon. At (*A*) EW12, (*B*) EW14, and (*C*) EW16 coexpression of TuJ1 and Sub P was observed in cells within ganglia-like structures at the level of the myenteric plexus (*arrows*). In addition, TuJ1^{+} cells not expressing Sub P were observed (*arrowheads*). Scale bars, 25 μm.

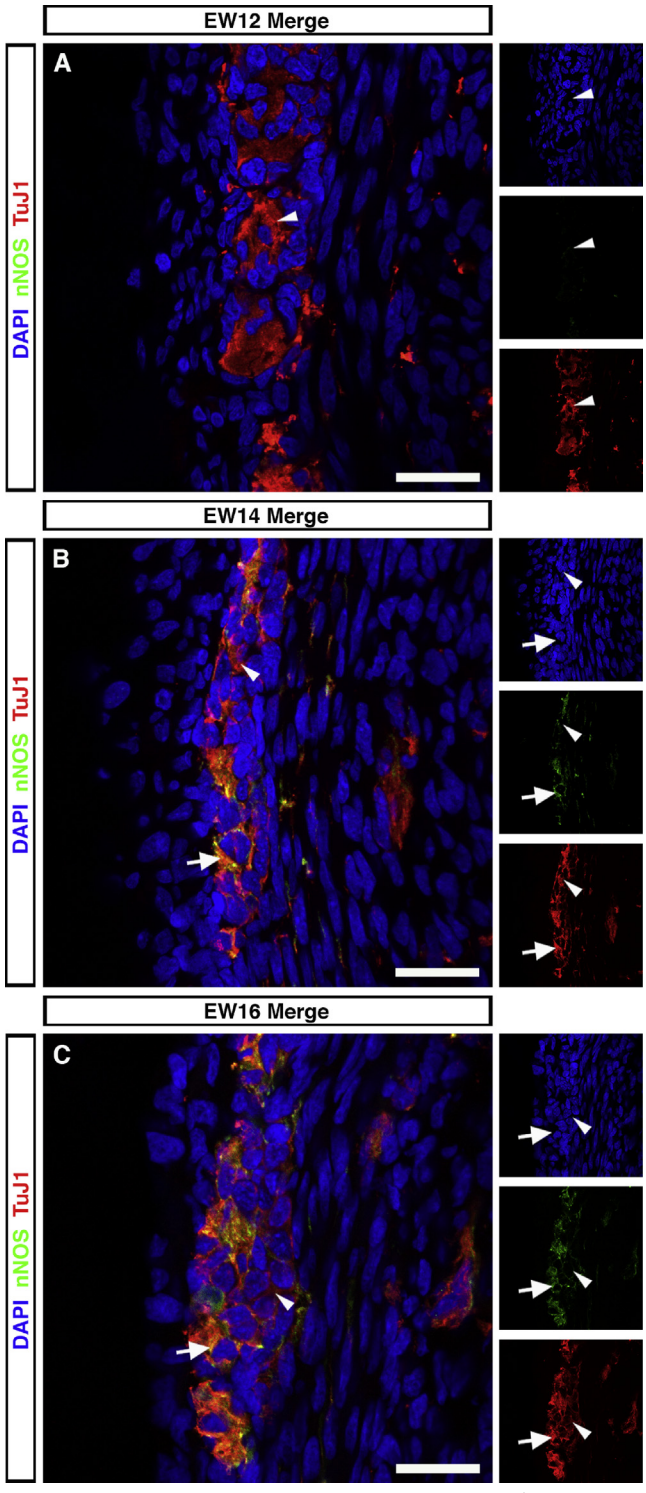

Supplementary Figure 3. Development of nNOS^{+} neurons in the human fetal colon. (*A–C*) Representative high-power immunofluorescent images showing expression of TuJ1 (*red*), nNOS (*green*), and DAPI (*blue*) in the developing fetal colon. At (*A*) EW12, TuJ1 expression was observed alone with no evidence of nNOS expression. At (*B*) EW14 and (*C*) EW16, coexpression of TuJ1 and nNOS was observed in cells in ganglia-like structures at the level of the myenteric plexus (*arrows*). In addition, TuJ1^{+} cells not expressing nNOS were observed (*arrowheads*). Scale bars, 25 μm.

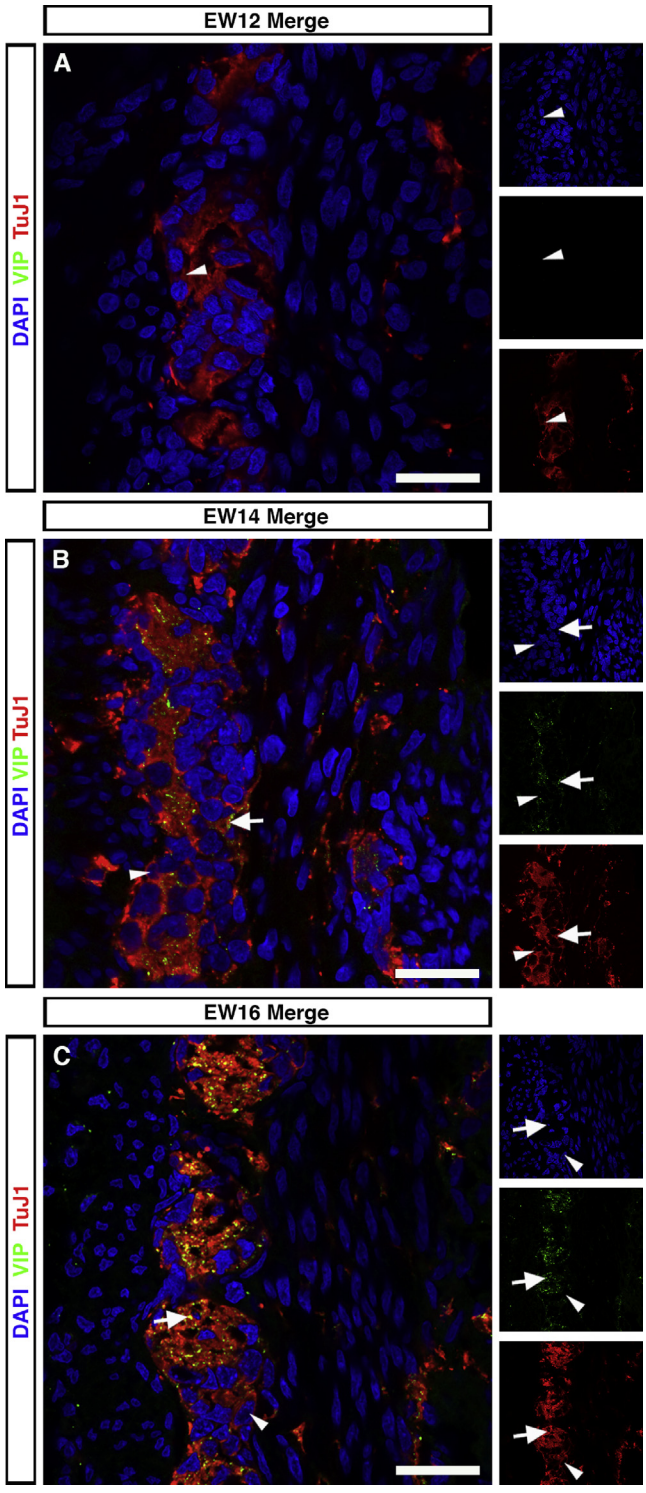

Supplementary Figure 4. Development of VIP^{+} neurons in the human fetal colon. (*A–C*) Representative high-power immunofluorescent images showing expression of TuJ1 (*red*), VIP (*green*), and DAPI (*blue*) in the developing fetal colon. At (*A*) EW12, TuJ1 expression was observed alone with no evidence of VIP expression. At (*B*) EW14 and (*C*) EW16, TuJ1^{+} cells, at the level of the myenteric plexus, were observed displaying punctate VIP expression (*arrows*). In addition, TuJ1^{+} cells not expressing VIP were observed (*arrowheads*). Scale bars, 25 μm.

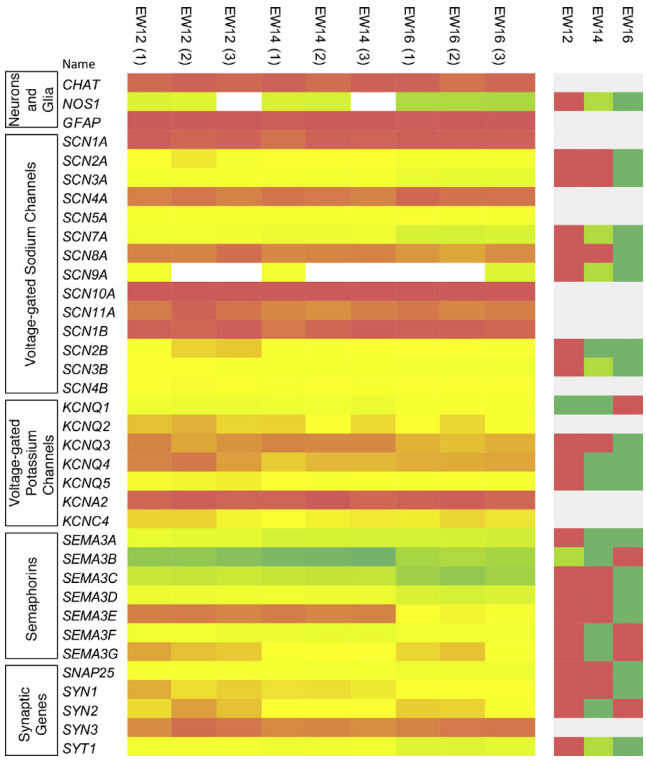

Supplementary Figure 5. Representative gene expression heatplot for candidate genes in the human fetal colon. Heatplot based on RNA sequencing analysis (stringent analysis parameters) of individual fetal colon samples, showing gene expression (*left*) at EW12, EW14, and EW16 [low relative expression (red) and high relative expression (*green*)]. Average expression by time point (*right*) shows directionality of expression from lower expression (*red*) to higher expression (*green*). Significant changes in gene expression represent false discovery rate values ≤ 0.05.

Supplementary Table 1. Primary Antibodies Used for Immunohistochemistry

Primary antibody	Concentration	Company
Mouse anti-TuJ1	1:500	BioLegend
Rabbit anti-TuJ1	1:500	BioLegend
Rabbit anti-SM22	1:1000	Abcam
Mouse anti-S100	1:100	Abcam
Goat anti-VAChT	1:200	Thermo Fisher Scientific
Rabbit anti-nNOS	1:400	Invitrogen
Mouse anti-Sub P	1:100	R&D Systems
Sheep anti-SNAP 25	1:200	R&D Systems
Mouse anti-Synaptophysin	1:250	Serotec

NOTE. Abcam, Cambridge, UK; BioLegend, San Diego, CA; Invitrogen, Waltham, MA; R&D Systems, Minneapolis, MN; Serotec, Oxford, UK; Thermo Fisher Scientific, Waltham, MA.

Supplementary Table 2. Secondary Antibodies Used for Immunohistochemistry

Secondary antibody	Alexa Fluor	Concentration	Company
Goat anti-mouse	488	1:500	Invitrogen
Goat anti-mouse	568	1:500	Invitrogen
Goat anti-rabbit	568	1:500	Invitrogen
Donkey anti-goat	488	1:500	Invitrogen
Donkey anti-sheep	488	1:500	Invitrogen
DAPI	—	1:1000	Sigma-Aldrich

NOTE. Invitrogen, Waltham, MA; Sigma-Aldrich, St Louis, MO.

Supplementary Table 3. Primers Used for qRT-PCR

Gene	Primer (5′–3′)
SCN2AF	TCCATGGAATTGGTTGGATT
SCN2AR	TTGTTTTCAATGCTCGGAGA
SCN3AF	TTCCTCTGGAAGGCAAAGAG
SCN3AR	AACCATGCATCACAGCAGTC
SCN5AF	CTCACCAACTGCGTGTTCAT
SCN5AR	CCTCGAGCCAGAATCTTGAC
SCN8AF	TGTGTGGCCCATAAACTTCA
SCN8AR	GCATCAGAACTGTTCCCACA
SCN9AF	CCCAACCTCAGACAGAGAGC
SCN9AR	TGGAGAGCAATTCCAGATCA
KCNQ2F	TCGTGCTGTCTGTGTTTTCC
KCNQ2R	ATCCGCACGAAGTACTCCAC
KCNQ3F	ATTCTGGCTGTCCTGACCAC
KCNQ3R	ACTCGGCTCCAAAGATGAAA
nNOSF	ACAGTCCCCCACAAAGAATG
nNOSR	GGAGCCCATGCAGATGTACT
SEMA3AF	AAGGGATCAGCCGTGTGTAT
SEMA3AR	CCTTGATAAGGCACCCATTG
SYN1F	GCCAATGGTGGATTCTCTGT
SYN1R	AACTGCGGTAGTCTCCGTTG
VIPF	GCTCCTTGTGCTCCTGACTC
VIPR	GGTTCATTTGCTCCCTCAAA
TAC1F	TGTTGGACTAATGGGCAAAA
TAC1R	TGTTGGACTAATGGGCAAAA
VAChTF	ACTATGCGGCCTCTGTTTTG
VAChTR	AATAGGAGATGTCGGCGATG
S100BF	ATTCTGGAAGGGAGGGAGAC
S100BR	TCCACAACCTCCTGCTCTTT
ACTBF	AACCGCGAGAAGATGACCC
ACTBR	GCCAGAGGCGTACAGGGATAG
GAPDHF	CGACCTTCACCTTCCCCAT
GAPDHR	TAAAAGCAGCCCTGGTGACC

Supplementary Table 4. Analysis of Candidate Gene Expression in the Human Fetal Colon

Gene	Relative Expression ± SD			*P* Value
	EW12	EW14	EW16	
SCN2A	0.004 ± 0.004	0.005 ± 0.005	0.005 ± 0.003	.888
SCN3A	0.009 ± 0.004	0.010 ± 0.006	0.013 ± 0.006	.433
SCN5A	0.002 ± 0.002	0.006 ± 0.005	0.003 ± 0.002	.128
SCN8A	0.003 ± 0.001	0.012 ± 0.015	0.006 ± 0.003	.233
SCN9A	0.026 ± 0.013	0.040 ± 0.025	0.056 ± 0.019	.056
KCNQ2A	0.001 ± 0.001	0.003 ± 0.003	0.002 ± 0.001	.228
KCNQ3A	0.001 ± 0.001	0.003 ± 0.003	0.002 ± 0.002	.305
nNOS	0.003 ± 0.002	0.013 ± 0.013	0.008 ± 0.002	.112
VAChT	0.002 ± 0.002	0.004 ± 0.005	0.003 ± 0.002	.591
TAC-1	0.276 ± 0.553	0.189 ± 0.335	0.713 ± 1.401	.563
VIP	0.757 ± 0.632	0.908 ± 0.376	2.559 ± 2.333	.080
S100B	0.217 ± 0.110	1.279 ± 1.420	0.469 ± 0.182	.101
SYN1	0.004 ± 0.006	0.004 ± 0.003	0.006 ± 0.003	.649
SEMA3A	0.057 ± 0.010	0.113 ± 0.080	0.101 ± 0.058	.237

NOTE. Comparison of the relative expression (mean ΔCT value ± SD) of candidate genes in the human fetal colon at EW12, EW14, and EW16, as analyzed by qRT-PCR. *P* values were calculated by Student *t* test.
SD, standard deviation.